CrystEngComm

Accepted Manuscript

ROYAL SOCIETY OF CHEMISTRY

www.rsc.org/crystengcomm

Cite this: DOI: 10.1039/c0xx00000x

www.rsc.org/crystengcomm

ARTICLE TYPE

Growth evolution of Si_xN_y on GaN underlayer and its effects on GaN-on-Si (111) heteroepitaxial quality

Tzu Yu Wang,[a] Sin Liang Ou,[a] Ray Hua Horng[b,c] and Dong Sing Wuu*[a,d]

Received 27th December 2013, Accepted Xth XXXXXXXXX 20XX

DOI: 10.1039/b000000x

The GaN epilayers were grown on Si(111) substrates via combining the techniques of AlN buffer, graded AlGaN structure and Si_xN_y interlayer by metalorganic chemical vapor deposition. The Si_xN_y interlayers with various growth time (t_g) of 0-60 s were introduced into the growth of GaN epilayers. To thoroughly realize the growth evolution of Si_xN_y, the measurements of atomic force microscopy, field emission scanning electron microscopy and nano-Auger electron spectroscopy were performed. From the measurement by transmission electron microscopy, it can prove that the nanocrystalline Si_xN_y was preferentially located at the dislocation cores and pits during growth process. For the fabrication of GaN/ graded AlGaN/AlN/Si, the full width at half maximum (FWHM) of XRD rocking curve at GaN(102) plane was reduced effectively from 965 to 771 arcsec with inserting the Si_xN_y into GaN epilayer, which resulted from the bending and annihilation of dislocations.

1. Introduction

For the applications of lighting and power devices such as blue and ultraviolet lighting emitting diodes, laser diodes and high electron mobility transistors, silicon carbide, sapphire and Si are the preferred substrates for nitride-based epilayer growth.[1-4] Among these substrates, Si wafer has higher superiority than the others due to its advantages of large size (> 6 inch), low cost and good thermal conductivity.[5] However, the melt-back etching between Ga and Si reacted at the growth process can result in a severe degradation of GaN quality.[6] Besides, the both large mismatches of thermal expansion coefficient (CTE, 116%) and lattice parameter (17%) between GaN and Si during cool-down process would lead to a high dislocation density of 10^9-10^{10} cm^{-2} in the epilayer.[7] It is well known that the optical and electrical properties of GaN-based devices are easily affected by these defects.[8] Fortunately, these problems can be solved by employing various buffer layers including AlN, graded $Al_xGa_{1-x}N$, AlN/GaN superlattice, low temperature AlN (LT-AlN), Si_xN_y interlayer and so on.[9-13] For the buffer techniques as mentioned above, the Si_xN_y interlayer is an effective method to reduce the dislocation density of GaN, which is also called the SiN_x nanomask or SiH_4 treatment by inducing the silane, disilane (Si_2H_6) and tetraethyl-silicon (TESi) as the Si source.[14,15] Via using the Si_xN_y interlayer, it not only causes the transformation of growth mode for regrowth GaN from three-dimension (3D) to two-dimension (2D), but also results in the annihilation and bending of threading dislocations (TDs).[16] Most of studies have demonstrated that the improvement in crystal quality of GaN epilayer and the reduction in dislocation density by inserting a Si_xN_y interlayer.[13-30] Additionally, Riemann et. al. have performed a series of experiments to analyze the characteristics of GaN-on-Si material system via the insertion of a SiN interlayer.[31] Their work presents not only the optical and structural properties of GaN overlayers grown on the SiN interlayers with various growth time but also the cathodoluminescence and micro-Raman results of GaN epilayer. Nevertheless, so far, both the growth evolution of Si_xN_y interlayer and its effect on the surface morphology of GaN are not completely clear. In this study, the correlations between the elements distribution, surface morphology and crystal structure of Si_xN_y interlayer on GaN underlayer have been investigated in detail, and the growth evolution of Si_xN_y interlayer can be established. Then the Si_xN_y interlayer with appropriate growth time was selected for the improvement in GaN epilayer quality via the combination of AlN and graded AlGaN buffer layers. In order to thoroughly realize the growth evolution of Si_xN_y interlayer, the Si_xN_y deposited with various growth time (t_g) of 0-60 s were prepared by metalorganic chemical vapor deposition (MOCVD) on the GaN layer. The growth evolution of Si_xN_y interlayer was investigated in detail via the measurements of field emission scanning electron microscopy (FESEM), atomic force microscopy (AFM), nano-Auger electron spectroscopy (nano-AES) and transmission electron microscopy (TEM). Except for the dislocation types observed by TEM, we also performed the high resolution TEM (HR-TEM) measurement to prove the existence of Si_xN_y interlayer in GaN-on-Si structure.

2. Experimental

The epilayer structures in this study were grown on 2-inch Si(111) wafers by employing Aixtron 200/4 RF-S MOCVD system. H_2 was used as the carrier source during growth process. The ammonia (NH_3), silane (SiH_4), trimethyl aluminum (TMAl) and trimethyl gallium (TMGa) were utilized for N, Si, Al and Ga sources, respectively. Before the epilayer growth, the Si wafer

was heated at 1000 °C in H_2 ambient for 10 min to clean its surface. Fig. 1 shows the epilayer structures in our work. Firstly, the AlN nucleation layer and high temperature AlN (HT-AlN) layer were grown at 1000 and 1100 °C, respectively. To investigate the growth evolution of Si_xN_y, the Si_xN_y layers (grown at 1050 °C) with various t_g of 0-60 s were prepared on 250-nm-thick GaN layers deposited on the HT-AlN, as shown in Fig. 1(a). Then, the 750-nm-thick regrowth GaN layers were further grown on the structures (shown in Fig. 1(a)) to obtain the optimum t_g of Si_xN_y for GaN epilayer, as shown in Fig. 1(b). For the sake of improvement in GaN quality, we also adopted the technique of graded AlGaN layers. The three graded AlGaN layers with the thicknesses of 170, 270 and 460 nm were prepared, while the Al contents of these AlGaN were 70%, 50% and 20%, respectively. Next, the Si_xN_y layer with the optimum t_g was combined with graded AlGaN to grow the GaN epilayer. The 1.61-μm-thick GaN epilayers grown on graded AlGaN without and with the introduction of Si_xN_y interlayer into the GaN were exhibited in Fig. 1(c) and (d), respectively. The epilayer structures shown in Fig. 1(a)-(d) were denoted as samples A-D, respectively, for further discussions. It can be noted that the growth parameters of GaN for all samples were the same. Surface element distribution, Auger chemical state and depth profile of samples were analyzed by nano-AES. The crystal qualities of GaN films were determined by X-ray diffraction (XRD). Surface morphologies and roughnesses of samples were demonstrated by FESEM and AFM, respectively. Detailed structure and dislocation distribution in samples were observed by TEM.

3. Results and discussion

To investigate the influences of Si_xN_y with various t_g on sample surface, the surface morphologies of sample A with various t_g were observed by FESEM, as shown in Fig. 2. Before the discussion, we should clarify that the Si_xN_y nanoparticles with very small size were distributed uniformly on the GaN surface as the t_g was increased from 5 to 45 s. Meanwhile, these nanoparticles were gradually merged to form a Si_xN_y thin film with the thickness about 1.5 nm on the GaN surface with increasing the t_g to 60 s. These results will be displayed and discussed later by AES measurements. We can find that the sample A with t_g of Si_xN_y at 5 s presented a flat surface with few nano-pits (Fig. 2(a)). As the t_g of Si_xN_y was raised to 15 s (Fig. 2(b)), the pit amount was increased and combined with the other pits in the vicinity. Apparently, the separated grains with distinct boundaries appeared in the samples with further increasing the t_g of Si_xN_y to 25-30 s, as displayed in Fig. 2(c) and (e). Meanwhile, the significant difference in surface roughness between sample B with t_g of Si_xN_y at 25 and 30 s can be observed by 45º tilt, as shown in Fig. 2(d) and (f). There are two possible reasons to explain this surface phenomenon. Firstly, because the bond strength of Ga-N (103 kJ/mol) was lower than that of Si-N (439 kJ/mol),[32] the N atoms would be lost from GaN surface during high-temperature process and the Ga atoms were migrated to recombine with N from NH_3 source in the Si_xN_y growth. Secondly, the sticking coefficient of the migrated Ga atoms on Si_xN_y region was lower than that on GaN region, which resulted in an increment of restricted Ga adatoms in GaN

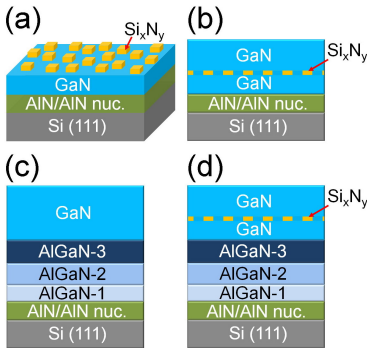

Fig. 1. Schematic illustrations for epilayer structures on Si(111) of (a) Si_xN_y/GaN/AlN, (b) GaN/AlN with an insertion of Si_xN_y, (c) GaN/graded AlGaN/AlN, and (d) GaN/graded AlGaN/AlN with an insertion of Si_xN_y. These four structures were denoted as samples A, B, C and D, respectively.

underlayer within Si_xN_y region as the t_g was increased from 5 to 30 s. Consequently, the pits were formed on the sample surface, and the migrated Ga atoms would move to other GaN regions and aggregate. Based on the results, the surface roughness of sample A cannot be affected effectively via the formation of Si_xN_y interlayer. It suggested that the surface roughness of sample A mainly depended on the surface roughening of the GaN underlayer. Therefore, the Si_xN_y nanoparticles tend to deposit on these pit defects due to lower formation energy of critical nucleus in the pit than that on the flat.[28] Finally, the grains were started to merge with increasing the t_g of Si_xN_y from 45 to 60 s, and then the large pits were diminished (Fig. 2(g) and (h)). Besides, to demonstrate the influence of Si_xN_y on GaN surface, a contrasted sample prepared with the same condition without silane flow for t_g at 60 s was also observed by FESEM, as exhibited in Fig. 2(i). It was found that the flat surface appeared in Fig. 2(i), indicating the evolution of GaN surface was indeed affected by the addition of Si_xN_y with various t_g. Based on the results reported by Pakuta et. al., the coalescing hill-like growth of GaN epilayer would lead

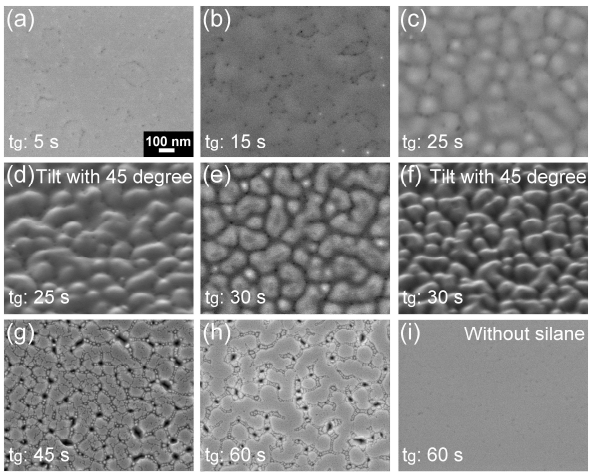

Fig. 2. Top view FESEM images for sample A with t_g of Si_xN_y at (a) 5 s, (b) 15 s, (c) 25 s, (d) 25 s with 45º tilt, (e) 30 s, (f) 30 s with 45º tilt, (g) 45 s and (h) 60 s. (i) FESEM image for a contrasted sample prepared with the same condition without silane flow for t_g of 60 s.

to a rough surface, which can be owing to the etching of GaN by introducing silane during the Si_xN_y formation.[29] However, in our case, the changes in surface of sample A could be resulted from GaN migration via the restriction of Ga adatoms in GaN underlayer within Si_xN_y region and merging of Si_xN_y grains as the t_g was increased.

Except for the FESEM observation, the surface status of sample A with various t_g of Si_xN_y was also explored from 3D morphology and roughness by using AFM. Fig. 3(a)-(f) exhibits the AFM images of sample A with t_g of Si_xN_y at 5, 15, 25, 30, 45 and 60 s, respectively. At the t_g of 5 s (Fig. 3(a)), the root-mean-squared (RMS) value of 0.7 nm can be measured from a flat surface with few small pits. An obvious increment in roughness from 4.7 to 8.5 nm was found with increasing the t_g of Si_xN_y from 15 to 25 s (Fig. 3(b) and (c)), while the surface feature was transformed from numbers of large grains to massive hillocks and valleys. This could be considered that the GaN migration was restricted by Si_xN_y growth, leading to the surface morphologies in Fig. 3(b) and (c). Further increasing the t_g of Si_xN_y to 30 and 45 s, the RMS values were reduced to 4.3 and 2.9 nm, respectively, as seen in Fig. 3(d) and (e). Moreover, it can be found a lot of small grains appeared on the surfaces of these two samples. After growing the Si_xN_y for 60 s (Fig. 3(f)), the significant grain growth and merging on surface would cause the roughness increase to 5.2 nm. The result was consistent with FESEM image as presented in Fig. 2(h).

To identify the existence of Si_xN_y on the GaN layer, the nano-AES and TEM measurements were used in sequence. According to the nano-AES results, the Auger images for Si_xN_y with t_g of 5-10 s are non-clear, resulting from both too small Si_xN_y nanoparticles and the resolution limitation in AES measurement. Therefore, the Si_xN_y layers with t_g of 15-60 s grown on GaN were selected to compare their element distributions using nano-AES. Fig. 4(a), (b) and (c) show the surface morphology observed by SEM, elements distribution for Ga and Si via nano-AES for sample A with t_g of Si_xN_y at 15, 25, 45 and 60 s, respectively. With the t_g of Si_xN_y at 15-25 s, it can be seen that the rougher surface existed in the sample A. Further increasing the t_g to 45-60 s, the merged grains with many nano-pits were found in the sample. The Ga distribution maps shown in Fig. 4(b) revealed the Ga element appeared over the entire surfaces of samples, which implied the thickness of Si_xN_y was very thin. At the same time, the elemental Si was distributed homogeneously over the surface and increased gradually with the t_g of Si_xN_y, as displayed in Fig. 4(c). The increment in Si element was also performed from the enhancements both in brightness and intensity of distribution map.

Further confirmation for the binding state of Si on GaN layer was analyzed by Auger chemical spectrum. Fig. 5(a) exhibits the Auger spectrum of sample A with t_g of Si_xN_y at 60 s. According to our analyses, the peaks of C1, O1, N1, Ga1, Ga2, Ga3, Si1 and Si2 were detected from the sample surface. Among these elements, C1 and O1 were originated from adsorbed contaminations of C and O_2 in air, respectively. The Si1 (Si LVV) and Si2 (Si KLL) peaks located at the kinetic energies of 86 and 1616 eV can be identified in this spectrum. In comparison to the Auger peaks of pure elemental Si (93 and 1618 eV) and Si_3N_4 (84 and 1613 eV), it proved that the Si_xN_y compound was indeed formed on GaN epilayer.[33] Moreover, the result indicated that the composition of Si_xN_y was very close to Si_3N_4. The distributions of Ga, N and Si elements as a function of depth for the samples with t_g of Si_xN_y at 45 and 60 s were displayed in Fig. 5(b) and (c), respectively. At the t_g of 45 s, the atomic concentration of Si on the sample surface was only 3.4%, while an estimation for the thickness of Si_xN_y layer was less than 1 nm. With an increment of t_g to 60 s, the atomic concentration of Si on the sample surface was increased to 8.9%, as well as the Si_xN_y thickness of 1.5 nm can be achieved. These results were in good agreement with the maps of Si distribution shown in Fig. 4(c).

More direct evidences for the distribution of Si_xN_y on GaN layer were provided by the cross-sectional HR-TEM images displayed in Fig. 6. In the TEM images, the zone axis of GaN layer is [-1100]. Fig. 6(a) shows the cross-sectional TEM image of sample A with t_g of Si_xN_y at 25 s, where the interfaces of AlN/Si and GaN/AlN can be clearly identified. The thicknesses of AlN and GaN can be determined to 148 and 225 nm, respectively. In addition, there were some Si_xN_y nanoparticles deposited on the rough GaN surface. To investigate the Si_xN_y states on various positions of GaN surface, the HR-TEM images for regions 1 and 2 (marked in Fig. 6(a)) were presented in Fig. 6(b). For these two regions (1 and 2), the Si_xN_y nanoparticles

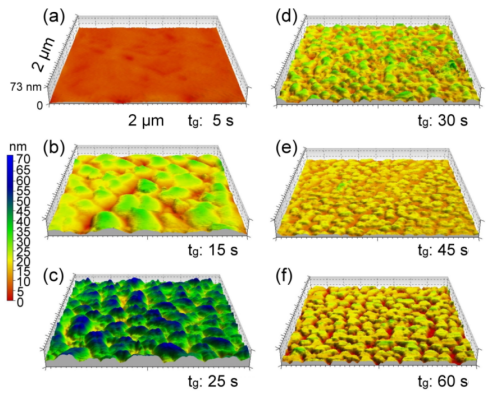

Fig. 3. AFM images of sample A with various t_g of Si_xN_y at (a) 5, (b) 15, (c) 25, (d) 30, (e) 45 and (f) 60 s.

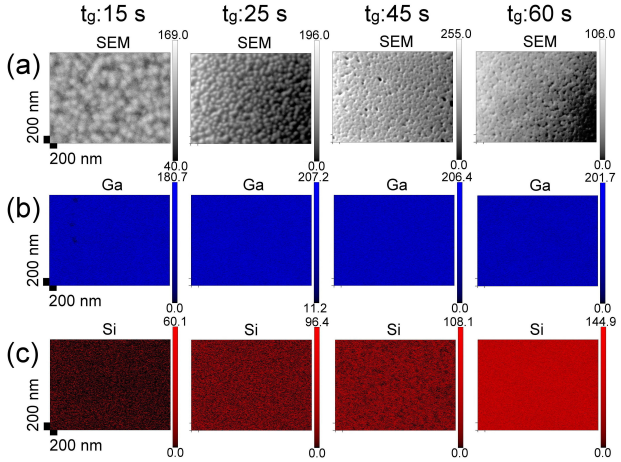

Fig. 4. (a) SEM images, elemental maps of (b) Ga and (c) Si for sample A with t_g of Si_xN_y from 15 to 60 s.

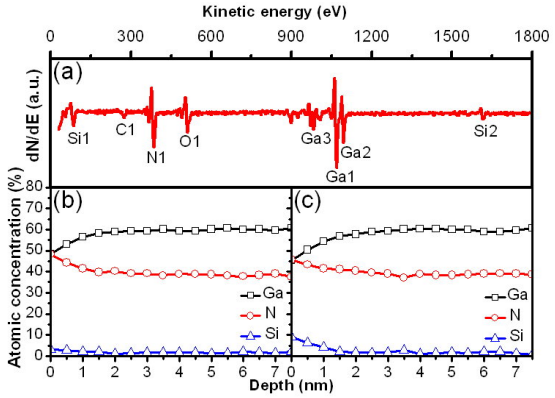

Fig. 5. (a) Auger spectrum of sample A with t_g of Si_xN_y at 60 s. Distributions of Ga, N and Si elements as a function of depth for sample A with t_g of Si_xN_y at (b) 45 and (c) 60 s.

were exactly located on the flat surface and dislocation, respectively. As the Si_xN_y was grown on flat plane (region 1), we can observe the non-continuous Si_xN_y with nanocrystallinity appeared on GaN surface, and its size was measured to about 0.9 nm. On the other hand, it was worth mentioning that the nanocrystalline Si_xN_y was easily bonded with the dislocation (region 2), which induced an obvious increase in Si_xN_y size to 6 nm. The results can forceful support the phenomenon about the preferential growth of Si_xN_y on dislocation cores. As shown in Fig. 6(c), there were few small pits on the flat surface with increasing the t_g of Si_xN_y to 45 s, and the thicknesses of AlN and GaN were 155 and 250 nm, respectively. Two various regions (1 and 2) marked in Fig. 6(c) were also further taken by HR-TEM to realize the Si_xN_y states on pit (region 1) and flat surface (region 2), respectively, as shown in Fig. 6(d). While the HR-TEM image was focused on the pit, we found that the nanocrystalline Si_xN_y with the size range of 4-6 nm was formed on the pit sidewall. It also can be observed that there is no substantial increase in the size of Si_xN_y nanoparticle with the increase in t_g. This phenomenon is attributed to the growth rate of Si_xN_y interlayer. Because the growth rate of Si_xN_y is very low, it is difficult to observe an obvious increase in the size of Si_xN_y nanoparticle with increasing the t_g from 25 to 45 s. On the contrary, the amount of Si_xN_y nanoparticle and the homogeneity of nanoparticle distribution are both improved as the t_g is increased from 25 to 45 s, especially for the Si_xN_y formation at the location of pits. In these HR-TEM images (Fig. 6(b) and (d)), the values of d-spacing for Si_xN_y nanoparticles were evaluated to be 2.40 and 1.95 Å, which corresponded to the (311) and (400) planes of cubic Si_xN_y structure, respectively. Besides, the space group of these Si_xN_y nanoparticles can be identified to Fd-3m.

From the element mapping and surface morphology results, the Si_xN_y interlayers with various t_g were homogeneously distributed on sample surface. Further detailed information on the structure and size of Si_xN_y nanoparticles obtained by TEM observation was used to correlate these results. Based on the results discussed above, the growth evolution of Si_xN_y grown on GaN with increasing the t_g was schematically illustrated in Fig. 7(a)-(g). As shown in Fig. 7(a), a flat GaN surface was formed at $t_g = 0$ s. The initial Si_xN_y nanoparticles were preferentially deposited on the dislocation cores and formed pits at $t_g = 5$ s (Fig. 7(b)). This is

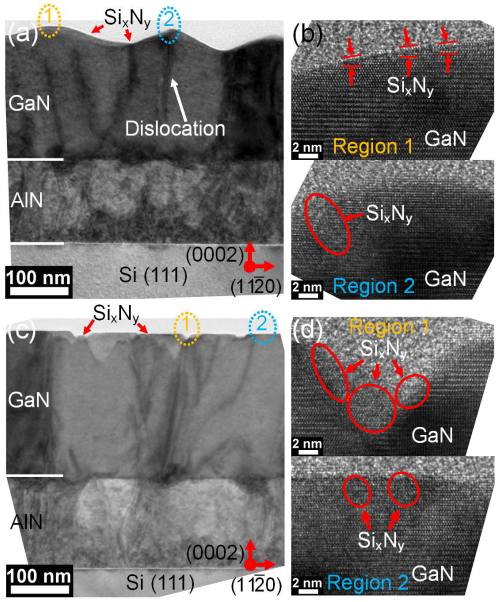

Fig. 6. Cross-sectional TEM images for sample A with t_g of Si_xN_y at (a) 25 and (c) 45 s. HR-TEM images for sample A with t_g of Si_xN_y at (b) 25 and (d) 45 s were focused on the sample surface, as marked in Fig. 7(a) and (c), respectively.

ascribed to the presence of N-dangling bonds at terrace and dislocation core, resulting in a preferential formation of Si_xN_y on the sites.[15] As the t_g was increased to 15 s, the pits and Si_xN_y nanoparticles were increased (Fig. 7(c)). At $t_g = 25$ s, due to an increase in the restricted Ga adatoms in GaN underlayer within Si_xN_y region, it resulted in the migration of Ga atoms to other GaN regions, and then the Ga atoms would aggregate. Therefore, the surface roughening of GaN underlayer was observed in Fig. 7 (d). At $t_g = 30$ s (Fig. 7(e)), the grain size and surface roughness of sample were both decreased, as confirmed in Fig. 2(f) and 3(d). This could be attributed to the excess distribution of Si_xN_y nanoparticles, inducing a significant increase in the restricted Ga adatoms in GaN underlayer. Contrarily, the result would lead to the decreases in both migration and aggregation of Ga atoms, forming a reduced surface roughness. Immediately, at $t_g = 45$ s, these excess Si_xN_y nanoparticles were assembled to aggregated islands with the size-reduced pits on the sample surface (Fig. 7(f)). Further increasing the t_g to 60 s, the aggregated grains were merged to form a thin film with the smaller pits, as presented in Fig. 7(g).

As we mentioned in sample B (Fig. 1(b)), the surface coalescence of regrowth GaN on Si_xN_y interlayers with various t_g was utilized to determine the optimum t_g. Fig. 8(a)-(e) presents the surface morphologies by FESEM of sample B with t_g of Si_xN_y at 5, 15, 25, 30 and 60 s, respectively. From our observation, the planar surface of regrowth GaN can be formed on the Si_xN_y with t_g of 5-25 s, as shown in Fig. 8(a)-(c). After growing the Si_xN_y for 5-25 s, there were more GaN regions appeared on the surface, which would accelerate the formation of planar surface as the regrowth process of GaN was performed. It can be assigned to the higher sticking coefficient of Ga on GaN region than that on Si_xN_y region. Furthermore, the incompletely coalesced surface with a lot of voids was observed in Fig. 8(d) as the t_g of Si_xN_y was risen to 30 s. In virtue of the abundant Si_xN_y formation with

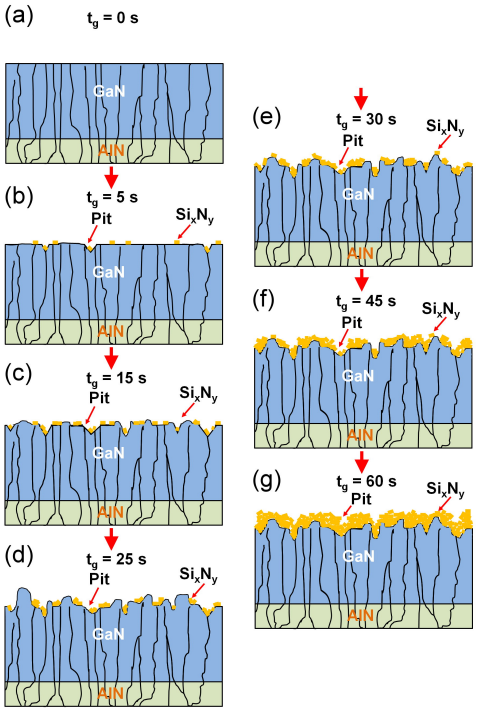

Fig. 7. Schematic illustrations for the growth evolution of Si_xN_y with increasing the t_g from 0 to 60 s. (a) Initial flat surface of GaN epilayer, (b) preferential deposition of Si_xN_y nanoparticles on the dislocation cores and the formation of pits, (c) uniform distribution of Si_xN_y nanoparticles with an increment of t_g, (d) surface roughening of GaN layer, (e) excess distribution of Si_xN_y nanoparticles on GaN layer, (f) merging of grains with the size-reduced pits by assembling Si_xN_y nanoparticles and (g) formation of Si_xN_y thin film via merging the aggregated grains.

increasing the t_g to 60 s, it would lead to the difficultly lateral merging of regrowth GaN from a large distance between each grain, inducing more GaN islands on the sample surface (Fig. 8(e)).

Fig. 9 shows the RMS roughness and full width at half maximum (FWHM) of XRD rocking curve at (002) and (102) planes for sample B with various t_g of Si_xN_y. As the regrowth GaN epilayers were prepared on the Si_xN_y with t_g of 0, 5, 10, 15, 20, 25, 30 and 60 s, the RMS values were measured to 1.5, 2.1, 0.8, 0.8, 0.7, 1, 225 and 520 nm, respectively. The surface roughness was raised with increasing the t_g of Si_xN_y, corresponding to the surface morphologies shown in Fig. 8. Due to only a slight difference in FWHM value of GaN(002) plane between 663 and 719 arcsec with modifying the t_g of Si_xN_y, the change in FWHM value of GaN(102) plane is more important to evaluate the epilayer quality of regrowth GaN. For the t_g of Si_xN_y at 0, 5, 10, 15, 20, 25, 30 and 60 s, the FWHM values of GaN(102) plane were 1589, 1348, 1327, 1259, 1169, 971, 636 and 681 arcsec, respectively. As known to all, the XRD curve of GaN(002) plane is sensitive to the screw- and mixed-types of TDs. Additionally, the crystal quality of GaN determined by (102) plane curve was resulted from all types of TDs.[34] As discussed above, the distribution and thickness of Si_xN_y both increased with increasing the t_g. In comparison to the t_g at 25 s, the regrowth areas for GaN epilayer were decreased at the t_g of 30 s. The decrease in regrowth areas for GaN epilayer would lead to an

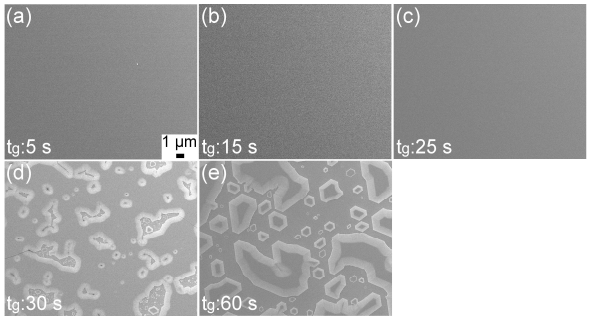

Fig. 8. Top view FESEM images for sample B with t_g of Si_xN_y at (a) 5, (b) 15, (c) 25, (d) 30 and (e) 60 s.

increment in coalescence distance between each GaN grain. This growth process is similar to the epitaxial lateral overgrowth (ELOG), which can cause a reduction in the density of TD by bending the dislocations. As displayed in Fig. 9, the epilayer quality of regrowth GaN was improved significantly with an increase of t_g from 25 to 30 s, revealing that the t_g of 30 s could be the critical point for the transformation of GaN growth to ELOG-like mode. In accordance with the previous research, an enhancement in crystal quality of GaN can be derived from a reduction in the density of TD by annihilating and bending the dislocations as the Si_xN_y interlayer was employed.[31] This is the reason why the FWHM value of (102) plane can be reduced effectively with increasing the t_g of Si_xN_y from 0 to 60 s. It deserved to be mentioned that the crack formation was created on the surface of sample B with t_g of Si_xN_y at 0-60 s as the thickness of regrowth GaN was increased to 1 μm, and this disadvantageous aspect was needed to solve urgently. Especially for the sample with t_g of Si_xN_y at 30-60 s, the crack density was obviously higher than that at the t_g of 0-25 s. To obtain the flat surface in regrowth GaN with the t_g of Si_xN_y at 30 and 60 s, the corresponded thickness of regrowth GaN should be thicker than 1 μm at the same growth condition. Therefore, the total thickness of GaN epilayer on AlN/Si would be increased to >2 μm, which was much higher than the critical thickness of GaN (1 μm) and then induced an increase in the crack density.[35] After taking into account the epilayer quality, surface roughness and crack status of sample B with various t_g of Si_xN_y, it indicates that the Si_xN_y interlayer with t_g of 15-25 s would be more suitable for GaN-on-Si structure. Moreover, from our measurement of strain state, it

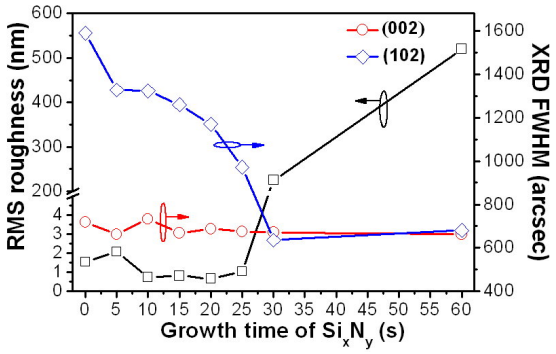

Fig. 9. Surface roughness and XRD FWHM values for GaN(002) and GaN(102) planes of sample B with various t_g of Si_xN_y from 0 to 60 s.

revealed that the sample B with t_g of Si_xN_y at 0-25 s possessed a higher tensile strain. Meanwhile, a relatively low tensile strain was formed in the sample B with t_g of Si_xN_y at 30 s due to its un-coalesced surface. With increasing the t_g to 60 s, the strain state of sample B became compressive because of the island growth. The results are similar to those in Riemann et. al. research.[31]

Despite of the significant improvement in epilayer quality of sample B, the practicability for device applications on these templates is still not enough. Consequently, further enhancement in the crystal quality of GaN epilayer and the elimination of surface cracks were both required, and the technique of graded AlGaN layer was used in our work. Moreover, to verify the additive effect on GaN quality by combining the Si_xN_y interlayer and graded AlGaN, the GaN epilayers (1.61 μm) grown on graded AlGaN without and with the introduction of Si_xN_y into GaN were both prepared to compare their qualities. These two structures were mentioned in Fig. 1 (1(c) and (d)) and defined as samples C and D, respectively. For the fabrication of sample D, the t_g of Si_xN_y was chosen to 15 s. The crystal quality and surface roughness of samples C and D were presented in Table 1. In these two samples, there existed similar results of RMS roughness (both of 0.6 nm) and XRD FWHM value for GaN(002) plane (536 and 540 arcsec). Nevertheless, in comparison to their XRD FWHM values for GaN(102) plane, it decreased from 965 to 771 arcsec as the t_g of Si_xN_y was increased from 0 to 15 s. This reveals the epilayer quality of GaN can be further enhanced via the combination of Si_xN_y interlayer and graded AlGaN techniques. In particular, there was almost no crack formed on the surface, even though the GaN thickness was increased to 1.61 μm, indicating the surface state was also improved remarkably. As presented in sample B without incorporating the Si_xN_y interlayer, it had a higher tensile strain and the surface crack. However, as the graded AlGaN was added (sample C), it exhibited a crack-free feature on the surface. This implies that the strain in the GaN-on-Si structure can be reduced significantly with adding the graded AlGaN.

Actually, the formation of surface crack can be attributed to both the differences in the lattice parameter and CTE between GaN and Si. However, because the cracks were always formed in the cool-down process, it revealed that the difference in the CTE was the main reason for the crack formation. The CTEs of GaN and Si were 5.59×10^{-6} and 3.59×10^{-6} K^{-1}, respectively. Therefore, a large tensile stress in GaN would be generated during the cool-down process. As the AlN and AlGaN buffer layers with smaller lattice parameters and CTEs than those of GaN were grown between Si substrate and GaN epilayer, the compressive stress in GaN was created and compensated the tensile stress. The thermal stresses (ε) of samples B and C were evaluated by using the following relation: $\varepsilon = \Delta\alpha(T_{growth}-T_{RT})$,[36,37] where the Δα is the difference in CTE (α) between the GaN film and underlayer, and T_{growth} and T_{RT} are growth temperature and room temperature, respectively. The α of AlGaN with 20% Al content was estimated to be 5.312×10^{-6} K^{-1} via the Vegard's law using the values for α(GaN) and α(AlN) of 5.59×10^{-6} K^{-1} and 4.2×10^{-6} K^{-1}, respectively. Thus, Δα of samples B and C can be calculated as follows: Δα(sample B) = α(GaN)-α(AlN) = 1.39×10^{-6} K^{-1} and Δα(sample C) = α(GaN)-α(AlGaN) = 2.78×10^{-7} K^{-1}. The tensile strains of GaN in samples B and C were 0.142% and 0.0287%, respectively. The significant reduction in tensile strain of GaN in sample C resulted in crack-free feature on the surface.

The TEM measurement was also performed on sample D to investigate the dislocation annihilation and quality improvement in GaN epilayer. The t_g of Si_xN_y inserted in sample D was selected to 15 s. Cross-sectional TEM image of sample D was displayed in Fig. 10(a), it can be found that various epilayers appeared in the GaN-on-Si structure. Then, the near Si_xN_y region marked in Fig. 10(a) was taken by HR-TEM image exhibited in Fig. 10(b). We can observe the nanocrystalline Si_xN_y grains with the size of 0.8 nm were non-continuously distributed in GaN epilayer. The cross-sectional TEM images with two beam

Table 1. Crystal qualities measured by XRD and surface roughnesses of samples C and D.

Table 1

Sample	t_g of Si_xN_y	XRD FWHM (002)	XRD FWHM (102)	RMS roughness
C	0 s	536 arcsec	965 arcsec	0.6 nm
D	15 s	540 arcsec	771 arcsec	0.6 nm

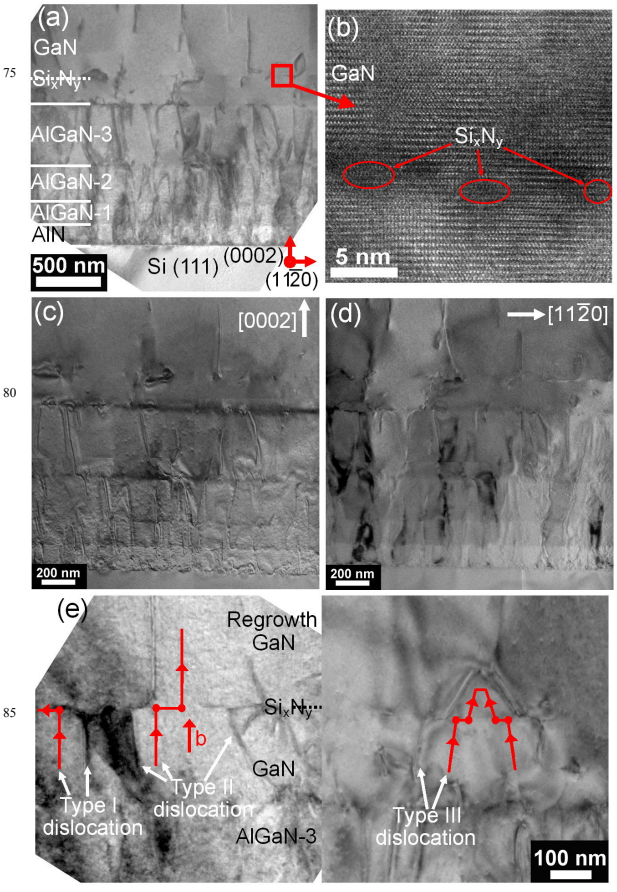

Fig. 10. (a) Cross-sectional TEM image for sample D with t_g of Si_xN_y at 15 s. (b) HR-TEM image taken at the Si_xN_y distribution in GaN epilayer marked in Fig. 10(a). TEM images with two perpendicular diffraction vectors along (c) **g**=[0002] and (d) **g**=[11-20]. (e) Three types of dislocation (types I, II and III) in the GaN epilayer of sample D.

conditions for two perpendicular diffraction vectors along g=[0002] and g=[11-20] were shown in Fig. 10(c) and (d), respectively. The invisibility criterion g·b=0 can be used to distinguish the different types of dislocations, where b is the Burgers vector. Based on this criterion, the screw- and mixed-type dislocations were visible with g=[0002]. Meanwhile, the edge- and mixed-type dislocations were visible with g=[11-20]. Therefore, as the mixed-type dislocations both appeared in these two images were confirmed, the screw- and edge-type dislocations can be clearly identified in Fig. 10(c) and (d), respectively. It was observed that most of dislocations were annihilated in graded AlGaN region. Then the edge-type dislocations can be further annihilated via the insertion of a Si_xN_y interlayer, as shown in Fig. 10(d). The screw and edge dislocation densities can be calculated from the following equations: $D_{screw} = \beta_{(002)}/9b^2_{screw}$, $D_{edge} = \beta_{(102)}/9b^2_{edge}$, total dislocation density = $D_{screw}+D_{edge}$,[38] where D_{screw} is the screw dislocation density and D_{edge} is the edge dislocation density. The $\beta_{(002)}$ and $\beta_{(102)}$ are the FWHM values of GaN(002) and GaN(102) planes, respectively, and b is the Burgers vector length (b_{edge} = 0.3189 nm and b_{screw} = 0.5185 nm). By using the equations, the total dislocation density of sample D was evaluated to be 3.69×10^9 cm^{-2}. Based on the observation of cross-sectional TEM image (Fig. 10(a)), the dislocation density of sample D was estimated to be 3.8×10^8 cm^{-2}. For the XRD measurement, both the dislocations formed in GaN underlayer and regrowth GaN layer were estimated for the dislocation density. Nevertheless, as the cross-sectional TEM image was used, only the dislocations formed in regrowth GaN layer were evaluated for dislocation density. This was the reason why the dislocation density obtained from the XRD result was much higher than that from the cross-sectional TEM image. Furthermore, the bending and annihilation of dislocation with the assistance of Si_xN_y interlayer were presented in three types of dislocation (types I, II and III), as provided in Fig. 10(e). For type I, it revealed that the Si_xN_y pinned the surface dislocation and then induced a line bending of dislocation to the basal plane. As observed in type II, the dislocation was also pinned by Si_xN_y. However, the dislocation underwent two successive bending and went back to the original growth direction. In type III, it consisted of two dislocations belonged to type II with the opposite Burgers vector (b). Besides, these two dislocations in type III would encounter to each other and form a dislocation loop. Obviously, the reduction in dislocation density was mainly ascribed to the mechanisms of types I and III through bending and annihilation. The phenomenon agreed well with the result proposed by Contras et. al.[30]

4. Conclusions

In summary, the GaN-on-Si structures were fabricated by metalorganic chemical vapor deposition. For the t_g of Si_xN_y at 15-25 s, the formation of rougher surface was due to the restriction of Ga adatoms in GaN underlayer within Si_xN_y region, and the migrated Ga atoms would move to other GaN regions and aggregate. At t_g = 30 s, the excess distribution of Si_xN_y nanoparticles would cause a significant increase in the restricted Ga adatoms in GaN underlayer. Contrarily, the result can induce the reductions in both migration and aggregation of Ga atoms, leading to the decrease in surface roughness. With increasing the t_g to 45-60 s, the smoother surface can be resulted from the Si_xN_y grain growth and merging. Moreover, the direct evidence from TEM measurement suggested that the nanocrystalline Si_xN_y preferred to reside at the locations of dislocation cores and pits on surface than that of flat region without dislocation. Further enhancement in crystal quality was achieved using the structure of GaN/graded AlGaN/AlN/Si with inserting the Si_xN_y layer. We can observe that it has almost no crack existed on the sample surface by employing this structure, even though the GaN thickness is risen to 1.61 μm. The XRD FWHM value for GaN(102) plane was reduced from 965 to 771 arcsec as the Si_xN_y with t_g of 15 s was inserted into GaN. Additionally, the dislocation in GaN epilayer can be bent and annihilated with an addition of Si_xN_y interlayer. The improvement in epilayer quality was mainly because of the line bending of dislocation to the basal plane and annihilation of dislocation.

Acknowledgements

This work was supported by the Ministry of Economic Affairs under Grant No. 102-E0605 and National Science Council (Taiwan, R.O.C.) under the Contract Nos. 101-2221-E-005-023-MY3 and 102-2622-E-005-006.

Notes and references

[a] *Department of Materials Science and Engineering, National Chung Hsing University, Taichung 40227, Taiwan, R.O.C. Fax: +886-4-22855046 ;Tel: +886-4-22840500 ext. 714*
E-mail: dsw@dragon.nchu.edu.tw
[b] *Institute of Precision Engineering, National Chung Hsing University, Taichung 40227, Taiwan, R.O.C.*
[c] *Advanced Optoelectronic Technology Center, National Cheng Kung University, Tainan 70101, Taiwan, R.O.C.*
[d] *Department of Materials Science and Engineering, Da-Yeh University, Changhua 51591, Taiwan, R.O.C.*

1 S. Nakamura, M. Senoh, S. Nagahama, N. Iwasa, T. Yamada, T. Matsushita, Y. Sugimoto and H. Kiyoku, *Jpn. J. Appl. Phys.*, 1997, **36**, L1059.
2 T. Oka and T. Nozawa, *IEEE Electron Device Lett.*, 2008, **29**, 668.
3 C. Y. Lu, E. Y. Chang, J. C. Huang, C. T. Chang and C. T. Lee, *Electron. Lett.*, 2009, **45**, 1348.
4 Z. Y. Li, M. H. Lo, C. H. Chiu, P. C. Lin, T. C. Lu, H. C. Kuo and S. C. Wang, *J. Appl. Phys.*, 2009, **105**, 013103.
5 A. Dadgar, J. Blasing, A. Diez, A. Alam, M. Heuken and A. Krost, *Jpn. J. Appl. Phys.*, 2000, **39**, L1183.
6 A. Krost and A. Dadgar, *Mater. Sci. Eng.*, 2002, **93**, 77.
7 J. Sun, J. Chen, X. Wang, J. Wang, W. Liu, J. Zhu and H. Yang, *Mater. Lett.*, 2007, **61**, 4416.
8 S. J. Rosner, E. C. Carr, M. J. Ludowise, G. Girolami and H. I. Erikson, *Appl. Phys. Lett.*, 1997, **70**, 420.
9 S. Raghavan and J. M. Redwing, *J. Appl. Phys.* 2005, **98**, 023514.
10 A. Able, W. Wegscheider, K. Engl and J. Zweck, *J. Cryst. Growth*, 2005, **276**, 415.
11 E. Feltin, B. Beaumont, M. Läugt, P. de Mierry, P. Vennéguès, H. Lahrèche, M. Leroux and P. Gibart, *Appl. Phys. Lett.*, 2001, **79**, 3230.
12 A. Dadgar, M. Poschenrieder, J. Bläsing, K. Fehse, A. Diez and A. Krost, *Appl. Phys. Lett.*, 2002, **80**, 3670.
13 M. J. Kappers, R. Datta, R. A. Oliver, F. D. G. Rayment, M. E. Vickers and C. J. Humphreys, *J. Cryst. Growth*, 2007, **300**, 70.
14 A. Chakraborty, K. C. Kim, F. Wu, J. S. Speck, S. P. DenBaars and U. K. Mishra, *Appl. Phys. Lett.*, 2006, **89**, 041903.
15 S. Tanaka, M. Takeuchi and Y. Aoyagi, *Jpn. J. Appl. Phys.*, 2000, **39**, L831.
16 K. Cheng, M. Leys, S. Degroote, M. Germain and G. Borghs, *Appl. Phys. Lett.*, 2008, **92**, 192111.

17 J. Hertkorn, F. Lipski, P. Brückner, T. Wunderer, S. B. Thapa, F. Scholz, A. Chuvilin, U. Kaiser, M. Beer and J. Zweck, *J. Cryst. Growth*, 2008, **310**, 4867.

18 S. Fritze, P. Drechsel, P. Stauss, P. Rode, T. Markurt, T. Schulz, M. Albrecht, J. Bläsing, A. Dadgar and A. Krost, *J. Appl. Phys.*, 2012, **111**, 124505.

19 S. E. Park, S. M. Lim, C. R. Leb, C. S. Kim and B. O, *J. Cryst. Growth*, 2003, **249**, 487.

20 H. Ashraf, D. V. SridharaRao, D. Gogova, D. Siche, R. Fornari, C. J. Humphreys and P. R. Hageman, *J. Cryst. Growth*, 2010, **312**, 595.

21 J. Xie, S. A. Chevtchenko, Ü. Özgür and H. Morkoç, *Appl. Phys. Lett.*, 2007, **90**, 262112.

22 J. Xie, Ü. Özgür, Y. Fu, X. Ni, H. Morkoç, C. K. Inoki, T. S. Kuan, J. V. Foreman and H. O. Everitt, *Appl. Phys. Lett.*, 2007, **90**, 041107.

23 X. L. Fang, Y. Q. Wang, H. Meidia and S. Mahajan, *Appl. Phys. Lett.*, 2004, **84**, 484.

24 J. Hertkorn, P. Brückner, S. B. Thapa, T. Wunderer, F. Scholz, M. Feneberg, K. Thonke, R. Sauer, M. Beer and J. Zweck, *J. Cryst. Growth*, 2007, **308**, 30.

25 T. A. Rawdanowicz and J. Narayan, *Appl. Phys. Lett.*, 2004, **85**, 133.

26 E. Frayssinet, Y. Cordier, H. P. D. Schenk and A. Bavard, *Phys. Stat. Sol. C*, 2011, **8**, 1479.

27 A. Sagar, R. M. Feenstra, C. K. Inoki , T. S. Kuan, Y. Fu, Y. T. Moon, F. Yun and H. Morkoç, *Phys. Stat. Sol. (a)*, 2011, **202**, 722.

28 K. Y. Zang, Y. D. Wang, L. S. Wang, S. Y. Chow and S. J. Chua, *J. Appl. Phys.*, 2007, **101**, 093502.

29 K. Pakula, R. Bożek, J. M. Baranowski, J. Jasinski and Z. Liliental-Weber, *J. Cryst. Growth*, 2004, **267**, 1.

30 O. Contreras, F. A. Ponce, J. Christen, A. Dadgar and A. Krost, *Appl. Phys. Lett.*, 2002, **81**, 4712.

31 T. Riemann, T. Hempel, J. Christen, P. Veit, R. Clos, A. Dadgar, A. Krost, U. Haboeck and A. Hoffmann, *J. Appl. Phys.*, 2006, **99**, 123518.

32 T. S. Zheleva, O. H. Nam, M. D. Bremser and R. F. Davis, *Appl. Phys. Lett.*, 1997, **71**, 2472.

33 L. Yu and D. Jin, *Surf. Interface Anal.*, 2001, **31**, 338.

34 B. Heying, X. H. Wu, S. Keller, Y. Li, D. Kapolnek, B. P. Keller, S. P. DenBaars and J. S. Speck, *Appl. Phys. Lett.*, 1996, **68**, 643.

35 R. Luo, P. Xiang, M. Liu, T. Chen, Z. He, B. Fan, Y. Zhao, Y. Xian, Z. Wu, H. Jiang, G. Wang, Y. Liu and B. Zhang, *Jpn. J. Appl. Phys.*, 2011, **50**, 121001.

36 M. H. Kim, Y. G. Do, H. C. Kang, D. Y. Noh and S. J. Park, *Appl. Phys. Lett.*, 2001, **79**, 2713.

37 K. L. Lin, E. Y. Chang, Y. L. Hsiao, W. C. Huang, T. T. Luong, Y. Y. Wong, T. Li, D. Tweet and C. H. Chiang, *J. Vac. Sci. Technol. B*, 2010, **28**, 473.

38 J. H. Lin, S. J. Huang, Y. K. Su and C. W. Hsu, *J. Cryst. Growth*, 2013, **370**, 273.

Table of Contents entry

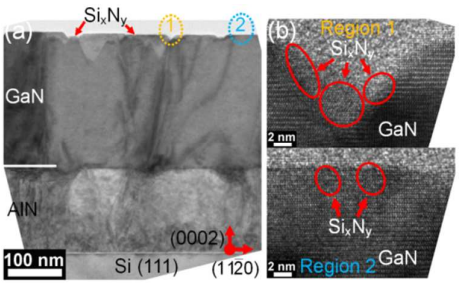

We verified that the nanocrystalline Si_xN_y with the size ranging from 4 to 6 nm appeared on the pit sidewall and preferred to reside at the pit.